Experimental Verification of a Multiuser Detection Technique for Asynchronous UOWC Systems

Weijie Liu, Xiaorui Chen, Nuo Huang, and Zhengyuan Xu, *Senior Member, IEEE*

***Abstract*—In this paper, a multiuser detection technique is proposed and experimentally verified in underwater optical wireless communication (UOWC) under dynamic channel conditions, which incorporates subspace-based delay estimation and decorrelating multiuser detection methods for an asynchronous access system. The subspace-based delay estimation method necessitates only prior knowledge of user spreading codes. The decorrelating multiuser detector can suppress multiple access interference (MAI) and demonstrates superior detection performance in a dynamic channel. An underwater testbench that supports three-user asynchronous access is established to further validate the multiuser detection technique. Experimental results demonstrate the effectiveness of alleviating the negative effects of user asynchrony, MAI, and intensity fluctuation.**

***Index Terms*—Underwater optical wireless communication (UOWC), asynchronous access, subspace-based delay estimation, decorrelating multiuser detection.**

I. Introduction

With the increasing number of underwater vehicles and sensors, as well as the rapid growth of underwater commercial and military applications, it is essential to establish a reliable, flexible and practical underwater wireless communication system [1]. Compared with conventional acoustic communication and radio frequency communication, underwater optical wireless communication (UOWC) has the advantages of low latency, low power consumption and high bit rate, thus can satisfy real-time communication and control applications [2]. Hitherto, most researches mainly focus on increasing the transmission distance, data rate, and robustness of the UOWC system [3], [4], [5]. However, investigation on underwater multiple access is rare, especially in the experimental aspect.

There are some pivotal issues in uplink multiple access under an underwater environment, such as user asynchronism, multiple access interference (MAI), near-far problem and dynamic channel state. In the absence of global time coordination, the issue of asynchronous transmission must be addressed in practical applications [6]. Asynchronous transmission of multiuser signals destroys the orthogonality between them and cause MAI. The misalignment of the light beam and variable transmission distance may lead to different received optical powers from different users, resulting in a near-far problem [7]. Meanwhile, various adverse factors in real underwater scenes, such as air bubbles and turbulence [8], can induce significant fluctuations in the underwater wireless optical channel, posing challenges to signal detection for multiuser communication. The work in [9] experimentally investigated the effects of air bubbles on the fluctuation in received signal intensity. It is observed that bubbles increase the dynamic range of the received signal intensity, thereby affecting interference cancellation in multiuser detection. Therefore, it is imperative to address the aforementioned issues in asynchronous uplink multiple access under a dynamic underwater environment to further enhance the applicability in a practical UOWC system.

There are several multiple access schemes, but not all of them are necessarily applicable to UOWC, and the choice of scheme is analyzed as follows. The conventional time division multiple access (TDMA) scheme is unsuitable for asynchronous uplink multiple access, as it necessitates a synchronous channel access [10]. Frequency division multiple access (FDMA) is not very suitable for optical communication due to the limited bandwidth of light emitting diodes (LEDs). For UOWC, only blue-green wavelengths exhibit low attenuation [11], limiting the availability of wavelength division multiple access (WDMA) and increasing implementation complexity. In contrast, code division multiple access (CDMA) [12] and non-orthogonal multiple access (NOMA) [13] are code-domain and power-domain multiple access techniques respectively that offer an advantage of high spectral efficiency. However, NOMA relies on successive interference cancellation (SIC) for symbol recovery [14], introducing a delay in each cancellation stage and leaving adequate room to explore the MAI reduction benefits for the first detected user. Recently, a SIC-free decoding method for NOMA was proposed to mitigate the error propagation [15]. This approach restricted the intensity relationship between two users and may not be well-suited for the dynamic underwater channel environment. Considering the anti-interference characteristics, asynchronous nature and multiuser detection techniques against near-far problem, CDMA emerges as a suitable choice for UOWC asynchronous access scenarios.

Optical CDMA has been widely investigated for indoor optical wireless communication and localization, and further

Manuscript received 8 December 2023; revised 2 February 2024; accepted 8 February 2024. Date of publication 13 February 2024; date of current version 27 February 2024. This work was supported in part by the National Key Research and Development Program of China under Grant 2022YFB2903400, in part by the Strategic Priority Research Program of CAS under Grant XDA22000000, and in part by the National Natural Science Foundation of China under Grant 62301525 and Grant 62101526. *(Corresponding authors: Nuo Huang; Zhengyuan Xu.)*

The authors are with the CAS Key Laboratory of Wireless-Optical Communications, School of Information Science and Technology, University of Science and Technology of China, Hefei 230027, China (e-mail: lwj1993@ustc.edu.cn; chenxr32@mail.ustc.edu.cn; huangnuo@ustc.edu.cn; xuzy@ustc.edu.cn).

Digital Object Identifier 10.1109/JPHOT.2024.3365695

extended to the UOWC system. For indoor optical wireless communication, Qian et al. proposed a scheme based on a multiple-LED structure to alleviate the nonlinearity of LEDs. Additionally, they introduced a CDMA scheme enabling multiple access with variable data rates [16]. In [17], the authors proposed an integrated visible light communication and positioning CDMA system. This system achieved a transmission rate of 1 Mbps and an average positioning error of 1.50 cm. In the case of UOWC, a UOWC system with compact smart transmitter and receiver prototype was successfully demonstrated within underwater unmanned vehicles [18]. Hassan et al. proposed two adaptive power control algorithms for the downlink underwater optical wireless networks incorporating an optical base station placed in the center of the cell and adopting a unique optical orthogonal code (OOC) [19]. In [12], a real-time prototype of an underwater optical wireless CDMA system was experimentally demonstrated, achieving a 115.2 Kbps reliable voice and video transmission. In [20], the performance of relay-assisted underwater optical wireless CDMA networks over turbulent channels was compared, where simultaneous and asynchronous data sharing among multiple users can be achieved with a unique OOC assigned to each user in the underwater optical network. Lyu et al. applied the spread spectrum technology in a UOWC system to further extend the transmission distance to 42 m with 6.68 attenuation length, and the minimum required signal-to-noise ratio (SNR) was reduced by 9 dB [21]. In [22], a quasi-omnidirectional transmitter was proposed and demonstrated for a CDMA-based UOWC system with four clients, achieving maximum data rates of 10 Mbps and 7.5 Mbps for each client over 10 m and 20 m underwater channels, respectively. Obviously, the existing works on underwater optical CDMA mainly focus on the channel capacity of point-to-point links and downlink synchronous links, as well as the analysis of underwater optical wireless CDMA networks without experimental verification.

This paper explores an asynchronous uplink CDMA-based UOWC scenario where various users communicate asynchronously with an access point (AP), and the channels exhibit dynamic behavior. We propose and experimentally test a multiuser detection technique that incorporates subspace-based delay estimation and a decorrelating detector in an underwater testbench with three-user access. During the experiment, a bubble generator is employed to emulate a bubbly channel with fluctuating signal intensity. The multiuser detection technique's capability to handle asynchronous access, MAI, and fluctuation is demonstrated and verified. The system achieves a bit rate of 2.0 Mbps per user.

The remainder of the paper is organized as follows. Section II introduces the system model, delay estimation and decorrelating detection methods. The experimental setup is elaborated in Section III. In Section IV, experimental results are presented to validate the feasibility of the asynchronous CDMA-based UOWC system. Finally, Section V concludes the paper.

II. System Model and Methodologies

In this section, the principle of asynchronous CDMA for UOWC is firstly introduced. Then, the subspace-based delay estimation method is briefly described and the details about the decorrelating-based multiuser detection method are provided.

A. System Model

Fig. 1 shows an underwater optical CDMA system based on intensity modulation/direct detection (IM/DD), where K users can communicate with the AP asynchronously. The information bit stream for each user is spread by a pseudo-noise (PN) sequence, and pulse shaping is utilized to suppress the inter-symbol interference (ISI). Subsequently, the generated alternating current (AC) signal and direct current (DC) bias are combined by a bias-T to drive the LED. After passing through the underwater channel, the superimposed optical signal of K users arriving at the receiver is converted into an electrical signal and sampled into a discrete digital signal by an analog-to-digital converter (ADC). Then, a multiuser detection method is introduced to further suppress or cancel the interference after accurately estimating the delay of each user.

The bit duration and chip duration are respectively denoted as T_b and $T_c = T_b/L$, where L is the spreading factor. Information bits "1" and "0" are mapped to "1" and "−1" for further analysis simplicity. Here, the intensity modulation scheme is considered. The electrical signal sent by the k-th user can be represented as

$$x_k(t) = \sum_{i=-\infty}^{\infty} P_k \, b_k[i] \, s_k(t - i\,T_b) + m_k, \tag{1}$$

where P_k denotes the amplitude of transmitted electrical signal, $b_k[i] \in \{+1, -1\}$ is the i-th transmitted bit, $s_k(t)$ is the spreading waveform which is zero outside the interval $[0, T_b]$, and m_k is the DC component. Then, the electrical signal at the transmitter is converted into the optical signal by the LED. The power loss in underwater channel is caused by optical beam divergence, water absorption and scattering. At the receiver, after photoelectric conversion and DC removal, the output electrical signal is sampled at time nT_s to yield the signal

$$r[n] = \sum_{k=1}^{K} \sum_{i=-\infty}^{\infty} A_k b_k[i] s_k\left[n - iLN_s - q_k\right] + w[n], \tag{2}$$

in which, K is the total number of users, $A_k = P_k h_k$ is the amplitude of received signal, where h_k is the equivalent channel gain comprising the electro-optical conversion, the channel attenuation, and the photoelectric conversion, $T_s = T_c/N_s$ denotes the sampling interval, N_s is the oversampling rate, $s_k[n] = s_k(nT_s)$ is the sample of spreading waveform, q_k represents the number of sample points corresponding to the delay, and $w[n]$ is the white Gaussian noise with zero mean and variance σ^2. For the subsequent analysis, the discrete sample vector of the spreading waveform of the k-th user is defined as

$$\boldsymbol{s}_k = \left[s_k[0], s_k[1], \ldots, s_k[LN_s - 1]\right]. \tag{3}$$

Clearly, the multiuser interference will degrade the communication performance of the target user, and an efficient multiuser detection technique needs to be proposed to achieve bit recovery.

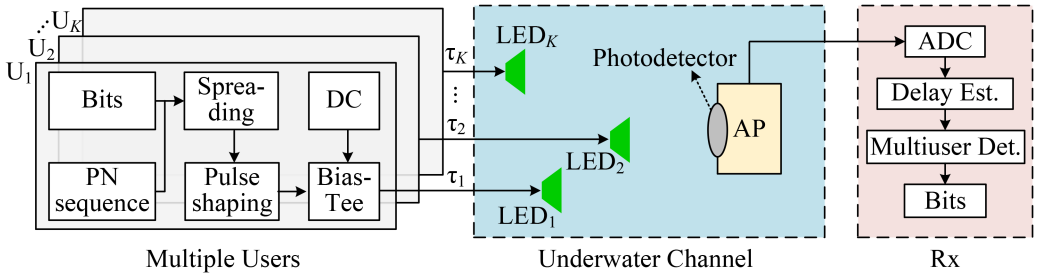

Fig. 1. Illustration of an asynchronous CDMA-based UOWC system.

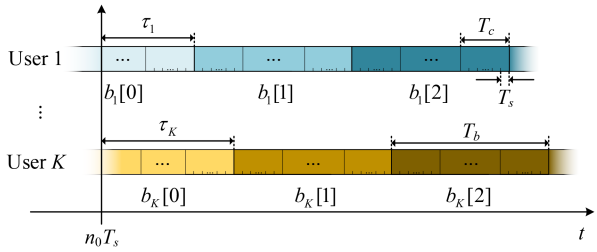

Fig. 2. Illustration of a K-user asynchronous access system.

B. Delay Estimation

To cancel MAI, the delay of each user needs to be estimated accurately. Sliding correlator is a conventional method for delay estimation, which works well in single user case or when the spreading waveforms are orthogonal [23]. However, it is not applicable in a near-far environment. Following the ideas of channel estimation and multiuser detection in the cellular CDMA systems [24], [25], a subspace-based blind delay estimation algorithm will be introduced to an asynchronous CDMA-based multiuser UOWC system, and the corresponding estimation results will be further fed into a decorrelating detector for multiuser detection.

Assume that the number of users as well as their spreading waveforms are known. Fig. 2 illustrates the received signal in a K-user asynchronous access system. Each user transmits information bits $\{b_k[i]\}$ asynchronously, and the received superimposed signal is sampled with initial time n_0T_s. The purpose of delay estimation is to determine the starting point of despreading for each user, represented by the time shift τ_k from n_0T_s to the beginning of the next bit of user k. If the delay exceeds one bit duration, it is constrained such that the delay modulo the bit duration is limited to be less than the bit duration, and the subspace-based delay estimation method remains applicable. Without loss of generality, we assume $\tau_k \in [0, T_b)$. The number of sample points corresponding to the delay is denoted as $q_k = [\tau_k/T_s]\text{mod}(LN_s)$, where $[\tau_k/T_s]$ represents the rounding operation of τ_k/T_s, and q_k takes values in the set $\{0, \ldots, LN_s - 1\}$.

Define the LN_s samples during the i-th bit duration as a vector $\boldsymbol{z}_i \in \mathbb{R}^{LN_s \times 1}$, which is written as

$$\boldsymbol{z}_i = [r[n_0 + iLN_s], \ldots, r[n_0 + (i+1)LN_s - 1]]^T. \quad (4)$$

Define vector $\boldsymbol{u}_k^r \in \mathbb{R}^{LN_s \times 1}$ to be the right side of $\boldsymbol{s}_k$ followed by zeros, and vector $\boldsymbol{u}_k^l \in \mathbb{R}^{LN_s \times 1}$ to be zeros followed by the left side of $\boldsymbol{s}_k$, i.e.,

$$\boldsymbol{u}_k^r = [s_k[LN_s - q_k], \ldots, s_k[LN_s - 1], 0, \ldots, 0]^T, \quad (5)$$

$$\boldsymbol{u}_k^l = [0, \ldots, 0, s_k[0], \ldots, s_k[LN_s - 1 - q_k]]^T. \quad (6)$$

The vector $\boldsymbol{z}_i$ can then be expressed as

$$\boldsymbol{z}_i = \boldsymbol{U}\boldsymbol{A}\boldsymbol{d}_i + \boldsymbol{w}_i, \quad (7)$$

where $\boldsymbol{U} = [\boldsymbol{u}_1^r, \boldsymbol{u}_1^l, \ldots, \boldsymbol{u}_K^r, \boldsymbol{u}_K^l] \in \mathbb{R}^{LN_s \times 2K}$, $\boldsymbol{A} = \text{diag}(A_1, A_1, \ldots, A_K, A_K) \in \mathbb{R}^{2K \times 2K}$, $\boldsymbol{d}_i = [b_1[i], b_1[i+1], \ldots, b_K[i], b_K[i+1]]^T \in \{+1, -1\}^{2K \times 1}$, and $\boldsymbol{w}_i \in \mathbb{R}^{LN_s \times 1}$ is the white Gaussian noise vector.

It is assumed that each user sends independent and identically distributed information bits, and the noise is independent of the useful signals. The covariance matrix of $\boldsymbol{z}_i$ can be estimated as

$$\hat{\boldsymbol{R}}_z = \frac{1}{M}\sum_{i=0}^{M-1} \boldsymbol{z}_i \boldsymbol{z}_i^T, \quad (8)$$

where M is the observation window size. The eigenvalue decomposition of $\hat{\boldsymbol{R}}_z$ can be represented as

$$\hat{\boldsymbol{R}}_z = \hat{\boldsymbol{V}}_s \hat{\boldsymbol{\Lambda}}_s \hat{\boldsymbol{V}}_s^T + \hat{\boldsymbol{V}}_n \hat{\boldsymbol{\Lambda}}_n \hat{\boldsymbol{V}}_n^T, \quad (9)$$

where $\hat{\boldsymbol{V}}_s \in \mathbb{R}^{LN_s \times 2K}$ is the eigenvector matrix corresponding to the first $2K$ eigenvalues of $\hat{\boldsymbol{R}}_z$ and $\hat{\boldsymbol{V}}_n \in \mathbb{R}^{LN_s \times (LN_s - 2K)}$ is the eigenvector matrix corresponding to the last $LN_s - 2K$ small eigenvalues of $\hat{\boldsymbol{R}}_z$. $\hat{\boldsymbol{V}}_s$ and $\hat{\boldsymbol{V}}_n$ span the signal subspace and noise subspace respectively. It is well known that signal subspace is orthogonal to noise subspace and the spreading waveform of each user lies in the signal subspace. However, it is difficult to satisfy $\hat{\boldsymbol{V}}_n^T \boldsymbol{U} = \boldsymbol{0}$ in practical implementation. Thus, quadratic programming can be used to estimate the delay as [25]

$$\hat{\tau}_k = \arg\min_{\tau_k \in [0, T_b)} \|\hat{\boldsymbol{V}}_n^T \boldsymbol{u}_k^r\|^2 + \|\hat{\boldsymbol{V}}_n^T \boldsymbol{u}_k^l\|^2. \quad (10)$$

The above minimization problem can be solved by traversing through all possible values of q_k to find the optimal value $\hat{q}_k$. The traversal requires LN_s searches for each user. Then the estimated delay of the k-th user is $\hat{\tau}_k = \hat{q}_k T_s$, which is further fed into a decorrelating detector for multiuser detection.

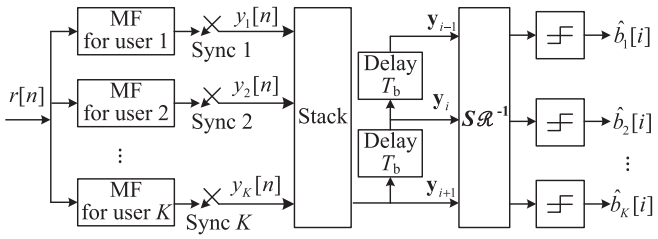

Fig. 3. Decorrelating detector for asynchronous CDMA.

C. Decorrelating Detection

Fig. 3 illustrates the principle of decorrelating detector [26], [27], [28], in which a linear transformation was applied to the matched filter (MF) outputs.

Assume the delays of users satisfy $0 \le \tau_1 \le \cdots \le \tau_K < T_b$. The output of each MF is sampled at the bit interval synchronized with the estimated user delay. For further derivation, define the cross-correlation matrix of the spreading waveforms at time lag m as $\boldsymbol{R}_m \in \mathbb{R}^{K\times K}$ whose (k,j)-th entry is given by

$$R_{k,j,m} = \sum_{n=-\infty}^{\infty} s_k[n-\hat{q}_k]s_j[n+mLN_s-\hat{q}_j]. \tag{11}$$

The output from MF for user k is represented as

$$y_k[n] = R_{k,k,0}A_k b_k[n] + \sum_{m=-1}^{1}\sum_{\substack{j=1\\ j\neq k}}^{K} R_{k,j,m}A_j b_j[n-m] + v_k[n], \tag{12}$$

where $v_k[n]$ is the noise from MF. Stacking $\{y_k[i]\}_{k=1}^K$ in a vector $\boldsymbol{y}_i = [y_1[i],\ldots,y_K[i]]^T \in \mathbb{R}^{K\times 1}$ for the i-th bit, it yields

$$\boldsymbol{y}_i = \boldsymbol{R}_1\boldsymbol{Q}\boldsymbol{b}_{i-1} + \boldsymbol{R}_0\boldsymbol{Q}\boldsymbol{b}_i + \boldsymbol{R}_{-1}\boldsymbol{Q}\boldsymbol{b}_{i+1} + \boldsymbol{v}_i, \tag{13}$$

where $\boldsymbol{b}_i = [b_1[i],\ldots,b_K[i]]^T \in \{+1,-1\}^{K\times 1}$, $\boldsymbol{Q} = \text{diag}(A_1,\ldots,A_K) \in \mathbb{R}^{K\times K}$, and $\boldsymbol{v}_i \in \mathbb{R}^{K\times 1}$ is the noise vector from MFs.

Clearly, the MAI mainly comes from the three adjacent bits of interfering users according to (13). In order to ensure the information bits of interest are included in the received data, MF outputs corresponding to three adjacent bits can be collected in a vector $y_i = [\boldsymbol{y}_{i-1}^T, \boldsymbol{y}_i^T, \boldsymbol{y}_{i+1}^T]^T \in \mathbb{R}^{3K\times 1}$ represented as

$$y_i = \mathcal{R}\mathcal{A}\mathcal{b}_i + \mathcal{v}_i, \tag{14}$$

where $\mathcal{R} \in \mathbb{R}^{3K\times 3K}$ is a block-Toeplitz matrix written as

$$\mathcal{R} = \begin{bmatrix} \boldsymbol{R}_0 & \boldsymbol{R}_{-1} & \boldsymbol{0} \\ \boldsymbol{R}_1 & \boldsymbol{R}_0 & \boldsymbol{R}_{-1} \\ \boldsymbol{0} & \boldsymbol{R}_1 & \boldsymbol{R}_0 \end{bmatrix},$$

$\mathcal{A} = \text{diag}(A_1,A_2,\ldots,A_K,\ldots,A_1,\ldots,A_K) \in \mathbb{R}^{3K\times 3K}$, $\mathcal{b}_i = [\boldsymbol{b}_{i-1}^T, \boldsymbol{b}_i^T, \boldsymbol{b}_{i+1}^T]^T \in \{+1,-1\}^{3K\times 1}$, and $\mathcal{v}_i$ includes the MF output noise as well as the interference coming from $\boldsymbol{b}_{i-2}$ and $\boldsymbol{b}_{i+2}$. For the i-th bit of each user, the output vector of decorrelating detector is represented as

$$\hat{\boldsymbol{b}}_i = \text{sgn}(\boldsymbol{S}\mathcal{R}^{-1}y_i) = \text{sgn}\left(\boldsymbol{S}(\mathcal{A}\mathcal{b}_i + \mathcal{R}^{-1}\mathcal{v}_i)\right), \tag{15}$$

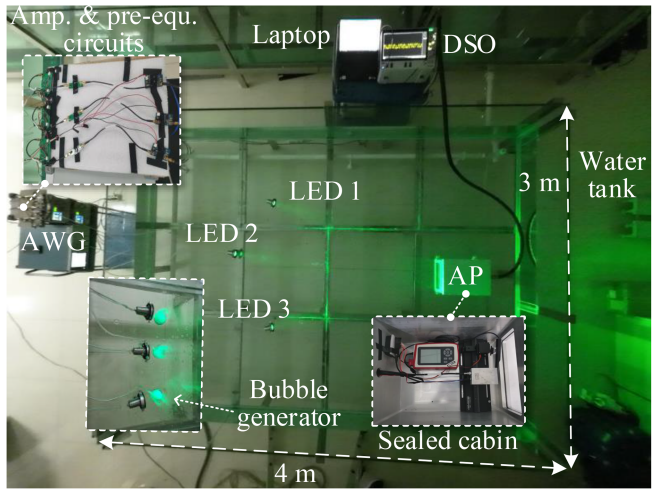

Fig. 4. Experimental setup.

where $\boldsymbol{S}$ is a selection matrix defined as

$$\boldsymbol{S} = \begin{bmatrix} \boldsymbol{0}_{K\times K} & \boldsymbol{I}_{K\times K} & \boldsymbol{0}_{K\times K} \end{bmatrix}.$$

Although a matrix inversion of $\mathcal{R}$ is required in the decorrelating detector, the corresponding computational complexity is reduced significantly as compared to that of the optimal multiuser detector [29]. From (15), the signal amplitudes of the users are not required for the decorrelating detector, which suggests that the decorrelating detector is suitable for an underwater environment with large dynamic signal range.

III. Experimental Setup and Preliminaries

Fig. 4 shows the experimental setup of the UOWC asynchronous CDMA system. A water tank of dimension 3 m × 4 m × 0.6 m is adopted to establish the underwater multiuser communication environment, where the attenuation coefficient of the filled tap water is measured to be 0.11 m^{-1} in the experiment. Three commercial green LEDs with central wavelength of 522 nm are separately sealed in three waterproof covers, and an avalanche photodiode (APD) (HAMAMATSU, C12702-11) with a circular photosensitive area of diameter 1.0 mm is encapsulated in an AP cabin. The three LEDs representing users $1\sim3$ and the APD representing the AP are all placed in the water tank. The LEDs transmit signals to the APD asynchronously. To simulate a dynamic UOWC environment, a bubble generator is positioned in front of each LED. The existence of air bubbles introduces varying levels of intensity attenuation along the transmission path. Here, user 1 is regarded as the desired user, and the other two users are considered as the interfering users.

At the transmitter of each user, a 5×10^4 pseudo-random binary sequence (PRBS) is generated in MATLAB as information bits, which is further spread by a pre-generated PN sequence with a spreading factor of 31. Here, the polynomials utilized in generating the PN sequence for three users are given as $g_1(x) = x^5 + x^3 + 1$, $g_2(x) = x^5 + x^4 + x^3 + x^2 + 1$ and $g_3(x) = x^5 + x^4 + x^2 + x + 1$. Each two of the three PN sequences form a preferred pair that has 3-valued cross-correlation

function [30]. After that, a square-root raised cosine filter with 10-time upsampling ratio is used as shaping filter, and the corresponding roll-off factor is fixed at 0.5. Then, the generated digital signals are loaded into an arbitrary waveform generator (AWG) (Tektronix, AWG5204) to produce the electrical signals with different bit rates. The output analog signal of each channel is delayed manually to simulate asynchronous transmission. The signals from AWG are amplified, pre-equalized and fed into self-designed bias-T circuits to drive the LEDs. The peak-to-peak voltage of the signal from AWG is 500 mV. The gain of the amplifier is 15.56 dB. The DC offset combined by the bias-T is 3 V. The pre-equalization circuit designed in our previous work is adopted to increase the bandwidth of each LED [31], leading to the chip rate 62.5 Mcps (cps represents chips per second) for a maximum data rate of 2.0 Mbps at a spreading factor 31. The sampling rates of the AWG are set to be 125 Msps, 312.5 Msps and 625 Msps to achieve the target chip rates 12.5 Mcps, 31.25 Mcps and 62.5 Mcps with 10-time upsampling ratio. The corresponding occupied bandwidths are 12.5 MHz, 31.25 MHz and 62.5 MHz, leading to bit rates 0.4 Mbps, 1.0 Mbps and 2.0 Mbps respectively.

At the receiver, a sealed cabin of AP containing an APD and optical power monitoring system is placed in the water tank. An optical power sensor (THORLABS, S130C) connected to an optical power meter (OPM) (THORLABS, PM100D) is placed in front of the APD, and is controlled by a servo to measure the incident optical power. The measured value of the optical power meter is further normalized by the sensitive area of the optical power sensor to obtain the received optical power per unit area. The output electrical signal from the APD is filtered by a 105 MHz low-pass filter (LPF) (Mini-Circuits, VLF-105+) to reduce the out-of-band noise. A digital storage oscilloscope (DSO) (Tektronix, MSO64B) is utilized to record the electrical signal for offline signal processing, which includes delay estimation, multiuser detection as well as calculation of error vector magnitude (EVM) and bit error rate (BER).

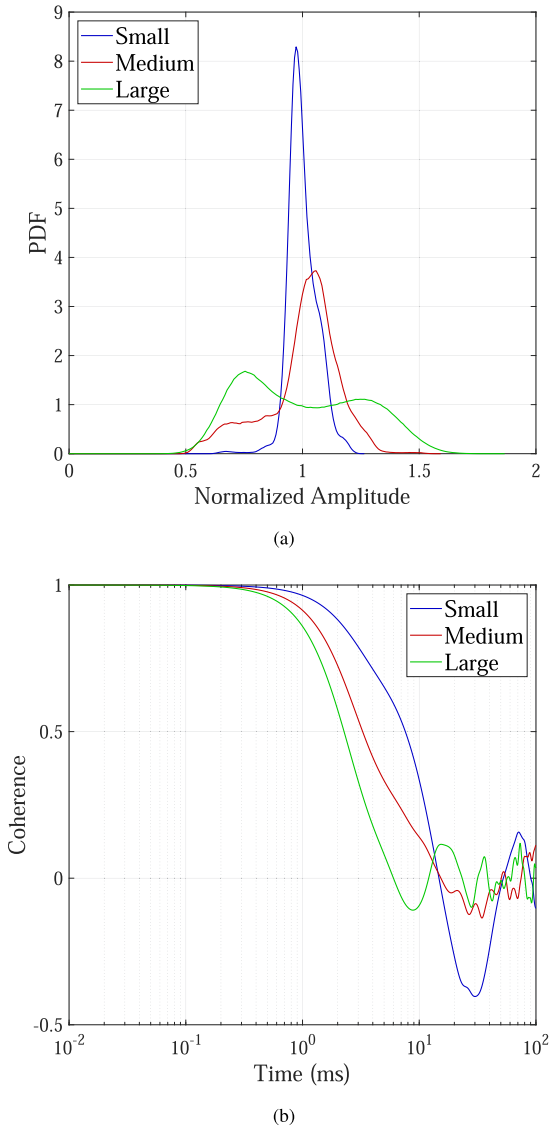

Fig. 5. Experimental results under three bubble flow rates. (a) Probability of normalized amplitude and (b) coherence time.

IV. Experimental Results and Discussions

In this section, the communication performances with different bit rates, delays, received optical powers and interfering optical powers under dynamic underwater conditions are thoroughly investigated and compared.

The bubble-induced underwater channel is firstly characterized. In the single LED case, a 1 MHz sinusoidal signal with 12.5 MHz sampling rate is sent when the received optical power in the static water is -0.199 dBm/mm^2. Then, the envelope of the sinusoidal signal is extracted as the amplitude of the signal. Three kinds of bubble flow rates (small, medium and large) controlled by the bubble generator are set in the experiments. Fig. 5(a) shows the probability density function (PDF) of amplitude fluctuation of received signal. The amplitude is normalized to make its expectation equal to one [8]. It can be seen that the dynamic range of signal intensity increases with the growth of the bubble flow rate, while the mean received signal intensity decreases. In Fig. 5(b), the temporal coherence characteristics of the dynamic channel induced by different bubble flow rates are depicted. The coherence time, measured as the 50-percentile value, is defined as the time interval for which the temporal correlation equals 0.5 [32]. The coherence times for small, medium, and large bubble flow rates are recorded as 7.6 ms, 3.3 ms, and 2.3 ms, respectively. Subsequent experimental results are obtained under the condition of the large bubble flow rate. All received optical powers are measured in static water.

Then, the performances of delay estimation under the large bubble flow rate condition are presented. In the experiment, user 2 and user 3 transmit their signals with fixed delays of $\tau_2 = 0.332T_b$ and $\tau_3 = 0.668T_b$. The signal from user 1 is transmitted at different delays, specifically $\tau_1 \in \{0.210T_b, 0.545T_b, 0.852T_b\}$. The received optical powers for both user 2 and user 3 are kept constant at -0.244 dBm/mm^2, while the received optical power of user 1 varies. For convenience of descriptions, the delay is normalized by bit duration T_b. Fig. 6 illustrates the absolute value of the normalized delay

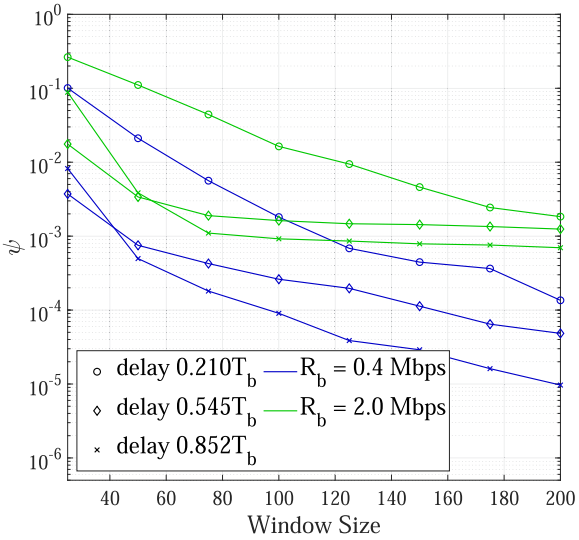

Fig. 6. Absolute value of normalized delay estimation error of user 1 versus the observation window size for received optical power -0.31 dBm/mm^2 under the large bubble flow rate condition.

estimation error ψ of user 1 versus the observation window size for various bit rates with a received optical power of -0.31 dBm/mm^2. The delay estimation error decreases as the observation window size increases, and a negligible delay estimation error can be observed when the observation window size exceeds 100. Consequently, a window size of 100 is adopted in the subsequent experiments, which is smaller than the coherence time for both bit rates of 0.4 Mbps and 2.0 Mbps.

Fig. 7 shows the probability distribution of the estimated delay normalized by T_b for user 1 with received optical power -0.31 dBm/mm^2 for bit rates 0.4 Mbps and 2.0 Mbps, respectively. The red dotted line represents the preset delay. The bin width of the histogram is equal to the sampling interval T_s. Obviously, the outputs of the delay estimation algorithm predominantly cluster around the preset delays, with an estimation error of no more than half a chip duration. Moreover, due to the signal distortion induced by the increase of bit rate, the variance of estimated delay at bite rate 2.0 Mbps is larger than that at bite rate 0.4 Mbps. These results affirm that the delay estimation algorithm performs effectively with an observation window size of 100, even in the near-far environment.

Subsequently, the communication performances of user 1 employing different detectors are further compared. A frame of data consists of a 5×10^4 PRBS. For each delay, a frame is generated and captured twice for BER evaluation. Therefore, there are a total of 3×10^5 bits for calculating the BER of user 1. The duration of a data frame exceeds the coherence time, resulting in signal intensity fluctuations within a frame of data. The proposed multiuser detection technique is implemented in the subsequent experiments. Conventional detector [33] and SIC detector [34] are employed as comparison benchmarks. The same APD is used at the AP in different experiments to ensure the same noise and receiver characteristics.

Fig. 8(a) shows the EVM performance versus received optical power of user 1 under various bit rates, while the received optical

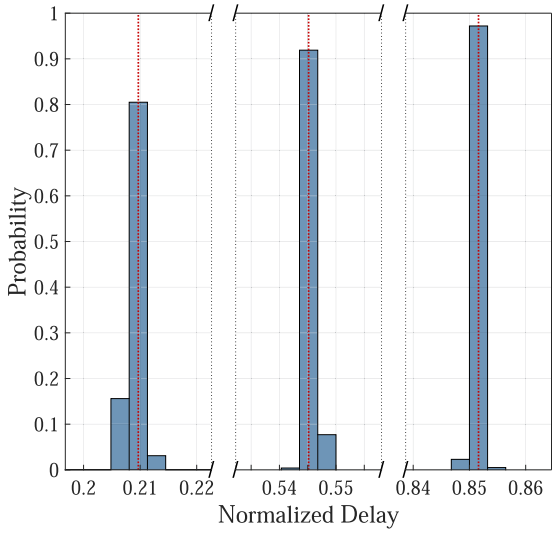

(a)

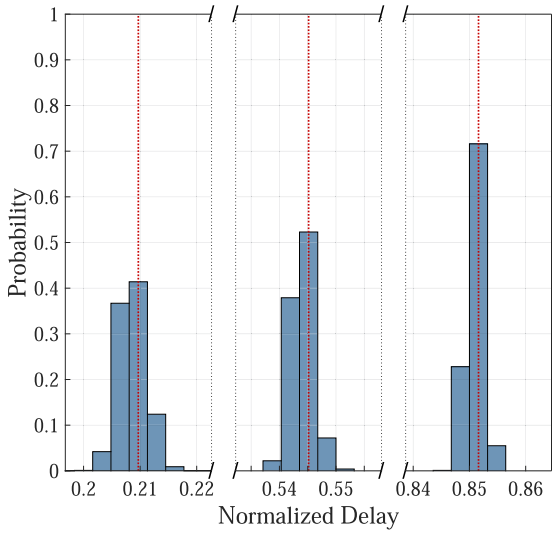

(b)

Fig. 7. Probability of estimated delay of user 1 normalized by T_b with observation window size 100 and received optical power -0.31 dBm/mm^2 for bit rates (a) 0.4 Mbps and (b) 2.0 Mbps under the large bubble flow rate condition.

powers of both user 2 and user 3 are fixed at -0.244 dBm/mm^2. Clearly, the EVM performances of conventional, SIC and decorrelating detectors improve with the increasing of the received optical power of user 1. The different received optical power between user 1 and the other two users implies that there is near-far problem, which impairs the performance of the conventional detector for user with weak signal (user 1). Both the SIC and decorrelating detectors outperform the conventional detector. Similar trends can be observed from the BER performances shown in Fig. 8(b). Note that the performance of the decorrelating detector surpasses that of the SIC detector. This is attributed to the fact that the SIC detector necessitates the estimation of signal amplitude for reconstructing the interference signal. In the experiment, first 100 bits of each frame are utilized to estimate the amplitude of each user signal. However, due to the influence

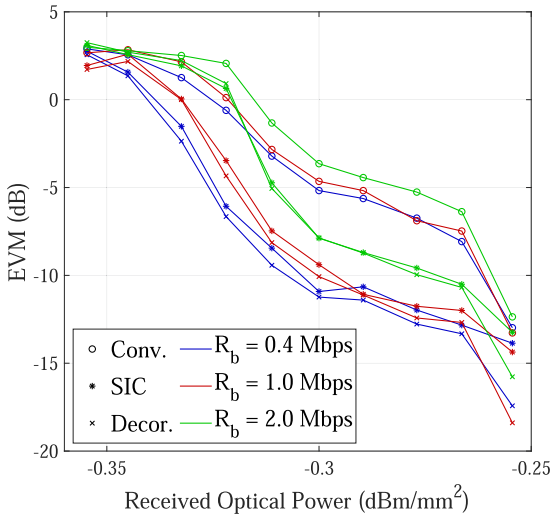

(a)

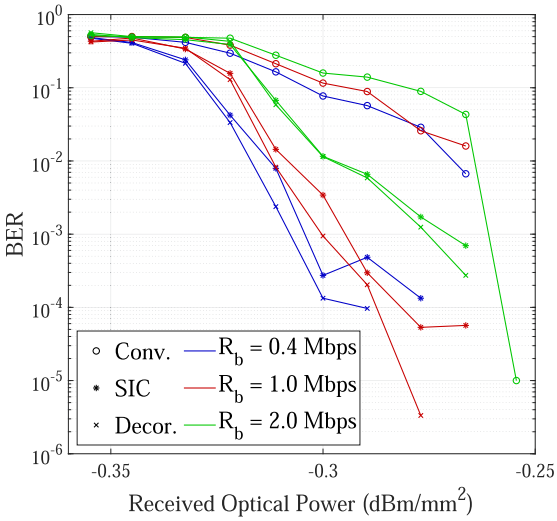

(b)

Fig. 8. EVM and BER of user 1 with two interfering users versus the received optical power of user 1 under the large bubble flow rate condition.

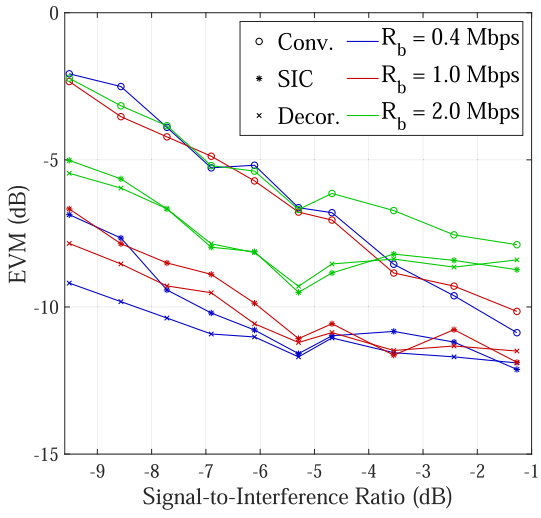

(a)

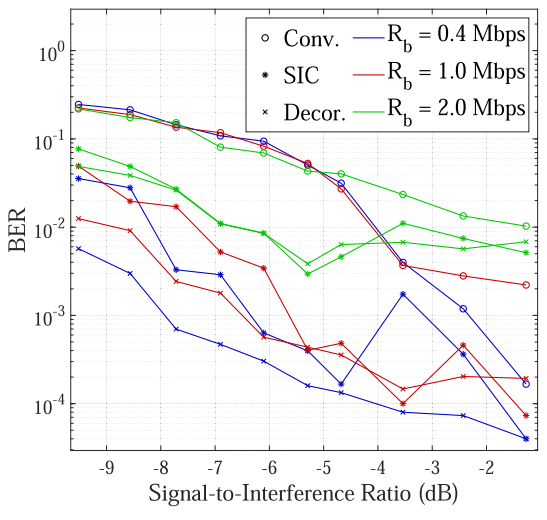

(b)

Fig. 9. EVM and BER of user 1 with two interfering users versus the signal-to-interference ratio under the large bubble flow rate condition.

of air bubbles, the signal amplitude of each user in a frame fluctuates. This imperfect amplitude estimation diminishes the potential performance gains. The superiority of the decorrelating detector, which does not require signal amplitudes, is evident.

To further investigate the impact of MAI, define the signal-to-interference ratio (SIR) as the ratio of the received optical power of user 1 to the sum of the received optical powers of interfering user 2 and user 3. The received optical power of user 1 is fixed at -0.299 dBm/mm^2. User 3 acts as one interfering user and its received optical power is the same as user 1. Therefore, the SIR varies with the received optical power of user 2. Fig. 9(a) shows the EVM performance of user 1 adopting different detectors versus the SIR ranging from -9.52 dB to -1.27 dB under various bit rates. Negative SIR values in the tested range represent severe MAI cases where the existence of a strong user exacerbates the MAI for the weaker user, commonly known as the near-far problem. The SIC and decorrelating detectors achieve a more stable EVM compared with the conventional detector, which verifies the feasibility of the SIC and decorrelating detectors in alleviating the near-far problem. Fig. 9(b) compares the BER performances of different detectors. The BER curves of the SIC detector exhibit large undulations compared to the BER curves of the decorrelating detector, and the BER is larger even in the case of low interference power. This behavior is attributed to changes in the detection order of the SIC detector. Even if user 1 and user 3 have the same received optical power in static water, air bubbles cause variations in their intensities. The SIC detector cancels signals in descending order of signal intensity. User with stronger signal that is detected earlier benefits less from the MAI reduction. The decorrelating detector can tolerate fluctuating intensity under a dynamic underwater environment. Meanwhile, It is observed that the BER encounters an error floor as the SIR increases. This is because as the received optical power of the interfering user 2 decreases, the SIR tends to be 0 dB, the

interference of user 3 and noise are dominant. Consequently, the signal to interference plus noise ratio of user 1 tends to be constant.

V. Conclusion

In this paper, an asynchronous CDMA-based UOWC system under dynamic channel is first experimentally demonstrated. Experimental results validate the feasibility of the subspace-based delay estimation and decorrelating multiuser detection methods in mitigating challenges associated with user asynchrony, near-far problems, and signal intensity fluctuations. The experiments highlight the efficacy of the subspace-based delay estimation algorithm in achieving accurate delay estimation. Furthermore, the decorrelating detector exhibits substantial performance gains over the conventional detector, particularly under conditions of severe MAI, surpassing the performance of the SIC detector in a dynamic underwater environment. The superior performance of the proposed multiuser detection technique is attributed to the synergistic integration of subspace-based delay estimation and the decorrelating detection. The experimental setup achieves a bit rate of 2.0 Mbps for each user, resulting in an aggregated rate of 6 Mbps for three users, while maintaining the BER below the forward error correction limit of 3.8×10^{-3} in an underwater asynchronous multiuser access scenario. It is noteworthy that the system can potentially support more users by increasing the spreading factor, albeit at the expense of increased processing cost.

References

[1] W. Liu, W. Jiang, N. Huang, and Z. Xu, "Experimental investigation of underwater optical wireless communication for correlated SIMO channel under temperature-induced turbulence," *IEEE Photon. J.*, vol. 15, no. 4, Aug. 2023, Art. no. 7302907.

[2] J. He, L. Xu, and Y. Xiao, "Performance comparison of different rotated QAM based DMT schemes in underwater optical wireless communication," *J. Lightw. Technol.*, vol. 41, no. 2, pp. 610–617, Jan. 2023.

[3] J. Du et al., "Experimental demonstration of 50-m/5-Gbps underwater optical wireless communication with low-complexity chaotic encryption," *Opt. Exp.*, vol. 29, no. 2, pp. 783–796, Jan. 2021.

[4] C. Fei et al., "100-m/3-Gbps underwater wireless optical transmission using a wideband photomultiplier tube (PMT)," *Opt. Exp.*, vol. 30, no. 2, pp. 2326–2337, Jan. 2022.

[5] W. Liu, Z. Ye, N. Huang, S. Li, and Z. Xu, "Multilevel polarization shift keying modulation for turbulence-robust underwater optical wireless communication," *Opt. Exp.*, vol. 31, no. 5, pp. 8400–8413, Feb. 2023.

[6] R. Diamant and L. Lampe, "Underwater localization with time-synchronization and propagation speed uncertainties," *IEEE Trans. Mobile Comput.*, vol. 12, no. 7, pp. 1257–1269, Jul. 2013.

[7] I. C. Ijeh, M. A. Khalighi, M. Elamassie, S. Hranilovic, and M. Uysal, "Outage probability analysis of a vertical underwater wireless optical link subject to oceanic turbulence and pointing errors," *J. Opt. Commun. Netw.*, vol. 14, no. 6, pp. 439–453, Jun. 2022.

[8] M. V. Jamali et al., "Statistical studies of fading in underwater wireless optical channels in the presence of air bubble, temperature, and salinity random variations," *IEEE Trans. Commun.*, vol. 66, no. 10, pp. 4706–4723, Oct. 2018.

[9] D. Chen, J. Wang, S. Li, and Z. Xu, "Effects of air bubbles on underwater optical wireless communication," *Chin. Opt. Lett.*, vol. 17, no. 10, Oct. 2019, Art. no. 100008.

[10] A. M. Abdelhady, O. Amin, A. Chaaban, B. Shihada, and M. S. Alouini, "Downlink resource allocation for dynamic TDMA-based VLC systems," *IEEE Trans. Wireless Commun.*, vol. 18, no. 1, pp. 108–120, Jan. 2019.

[11] Z. Zeng, S. Fu, H. Zhang, Y. Dong, and J. Cheng, "A survey of underwater optical wireless communications," *IEEE Commun. Surveys Tut.*, vol. 19, no. 1, pp. 204–238, First Quarter 2017.

[12] F. Akhoundi, J. A. Salehi, and A. Tashakori, "Cellular underwater wireless optical CDMA network: Performance analysis and implementation concepts," *IEEE Trans. Commun.*, vol. 63, no. 3, pp. 882–891, Mar. 2015.

[13] M. Jain, N. Sharma, A. Gupta, D. Rawal, and P. Garg, "Performance analysis of NOMA assisted underwater visible light communication system," *IEEE Wireless Commun. Lett.*, vol. 9, no. 8, pp. 1291–1294, Aug. 2020.

[14] L. Bariah, M. Elamassie, S. Muhaidat, P. C. Sofotasios, and M. Uysal, "Non-orthogonal multiple access-based underwater VLC systems in the presence of turbulence," *IEEE Photon. J.*, vol. 14, no. 1, Feb. 2022, Art. no. 7308707.

[15] X. Li et al., "Experimental demonstration of a real-time multi-user uplink UWOC system based on SIC-free NOMA," *Opt. Exp.*, vol. 31, no. 19, pp. 30146–30159, Aug. 2023.

[16] H. Qian, S. C. Dai, S. Zhao, S. Z. Cai, and H. Zhang, "A robust CDMA VLC system against front-end nonlinearity," *IEEE Photon. J.*, vol. 7, no. 5, Oct. 2015, Art. no. 7801809.

[17] D. Chen et al., "Integrated visible light communication and positioning CDMA system employing modified ZCZ and walsh code," *Opt. Exp.*, vol. 30, no. 22, pp. 40455–40469, Oct. 2022.

[18] J. A. Simpson, B. L. Hughes, and J. F. Muth, "Smart transmitters and receivers for underwater free-space optical communication," *IEEE J. Sel. Areas Commun.*, vol. 30, no. 5, pp. 964–974, Jun. 2012.

[19] N. B. Hassan, F. Akhoundi, and J. A. Salehi, "Adaptive power control algorithms in underwater wireless optical CDMA cellular networks," in *Proc. IEEE 4th Int. Workshop Opt. Wireless Commun.*, 2015, pp. 107–111.

[20] M. V. Jamali, F. Akhoundi, and J. A. Salehi, "Performance characterization of relay-assisted wireless optical CDMA networks in turbulent underwater channel," *IEEE Trans. Wireless Commun.*, vol. 15, no. 6, pp. 4104–4116, Jun. 2016.

[21] W. Lyu et al., "Experimental demonstration of an underwater wireless optical communication employing spread spectrum technology," *Opt. Exp.*, vol. 28, no. 7, pp. 10027–10038, Mar. 2020.

[22] X. Li et al., "Underwater quasi-omnidirectional wireless optical communication based on perovskite quantum dots," *Opt. Exp.*, vol. 30, no. 2, pp. 1709–1722, Jan. 2022.

[23] R. Pickholtz, D. Schilling, and L. Milstein, "Theory of spread-spectrum communications-A tutorial," *IEEE Trans. Commun.*, vol. 30, no. 5, pp. 855–884, May 1982.

[24] Z. Xu, P. Liu, and X. Wang, "Blind multiuser detection: From MOE to subspace methods," *IEEE Trans. Signal Process.*, vol. 52, no. 2, pp. 510–524, Feb. 2004.

[25] S. E. Bensley and B. Aazhang, "Subspace-based channel estimation for code division multiple access communication systems," *IEEE Trans. Commun.*, vol. 44, no. 8, pp. 1009–1020, Aug. 1996.

[26] K. S. Schneider, "Optimum detection of code division multiplexed signals," *IEEE Trans. Aerosp. Electron. Syst.*, vol. AES-15, no. 1, pp. 181–185, Jan. 1979.

[27] R. Kohno and M. Hatori, "Cancellation techniques of co-channel interference in asynchronous spread spectrum multiple access systems," *Elect. Commun. JPN (Part I: Commun.)*, vol. 66, no. 5, pp. 20–29, 1983.

[28] R. Lupas and S. Verdu, "Near-far resistance of multiuser detectors in asynchronous channels," *IEEE Trans. Commun.*, vol. 38, no. 4, pp. 496–508, Apr. 1990.

[29] S. Verdu, "Minimum probability of error for asynchronous Gaussian multiple-access channels," *IEEE Trans. Inf. Theory*, vol. 32, no. 1, pp. 85–96, Jan. 1986.

[30] R. Gold, "Maximal recursive sequences with 3-valued recursive cross-correlation functions," *IEEE Trans. Inf. Theory*, vol. 14, no. 1, pp. 154–156, Jan. 1968.

[31] Z. Yu, C. Gong, J. Wei, N. Huang, and Z. Xu, "3-Gb/s visible light communication over 5 m distance based on imaging system with low transmission power and off-the-shelf LEDs," in *Proc. Int. Wireless Commun. Mobile Comput. Conf.*, 2021, pp. 2109–2114.

[32] J. R. Hampton, *Introduction to MIMO Communications*. New York, NY, USA: Cambridge Univ. Press, 2014.

[33] S. Moshavi, "Multi-user detection for DS-CDMA communications," *IEEE Commun. Mag.*, vol. 34, no. 10, pp. 124–136, Oct. 1996.

[34] P. Patel and J. Holtzman, "Analysis of a simple successive interference cancellation scheme in a DS/CDMA system," *IEEE J. Select. Areas Commun.*, vol. 12, no. 5, pp. 796–807, Jun. 1994.